Geochemical Modeling of Two-Phase Flow with Interphase Mass Transfer

Craig F. Novak
Sandia National Laboratories, Albuquerque, NM 87185

Larry W. Lake
Dept. of Petroleum Engineering, University of Texas, Austin, TX 78712

Robert S. Schechter
Dept. of Chemical Engineering, University of Texas, Austin, TX 78712

Injecting an acidic aqueous solution into a carbonate-rich permeable medium can cause the formation of a mobile gas phase through mineral dissolution. The flowing gas can cause significant changes in mineral identities through interaction with the initially present mineral and aqueous species. We have developed a solution to such transport problems based on a finite difference implicit-pressure/explicit-saturation formulation for two-phase flow, using the local equilibrium assumption as calculated with the Villars-Cruise-Smith stoichiometric chemical equilibrium algorithm.

We illustrate the changes that occur to a calcite/iron (II) hydroxide medium upon injection of hydrochloric acid and the stripping of hydrogen sulfide gas from carbon dioxide gas injected into a siderite-rich medium. The examples demonstrate that the formation and/or presence of a gas phase can alter resident minerals and that minerals can remove impurities from a gas phase.

Introduction

Mineral alteration that occurs during transport through permeable media has implications in such diverse areas as well stimulation, groundwater contamination, hazardous waste containment and removal, and ore-body formation. When an aqueous phase flows into a permeable medium, some of the minerals initially present may dissolve and cause other minerals to precipitate. In the absence of significant dissipation, these reactions cause a series of concentration changes or *waves* that propagate with constant velocity (for uniform initial concentrations) and separate the medium into zones containing constant mineral concentrations. The fastest wave, the aqueous tracer wave, represents changes in the aqueous phase only and moves with the fluid velocity in single-phase flow.

Many researchers have studied a flowing aqueous phase interacting with soluble minerals (Bryant et al., 1986, 1987; Dria, 1988; Helfferich, 1989; Kirkner and Reeves, 1988; Lichtner, 1985, 1991; Novak et al., 1988; Ortoleva et al., 1987; Rege and Fogler, 1989; Rubin, 1983; Schechter et al., 1987; Walsh et al., 1982, 1984). As we do here, such flows are typically modeled as being in local thermodynamic equilibrium with constant physical properties and flow velocities. Moreover, most models assume that only the aqueous phase flows and do not allow a gas phase to form and flow. In an experimental study of a scale-removing chemical injected into a carbonate-containing Berea sandstone core, Simmons (1988) observed the production of a gas phase. This observation provides one motivation for this study.

Media with two simultaneously flowing phases are studied extensively in petroleum reservoir engineering and soil science, and many authors have examined two-phase flow as it relates to enhanced oil recovery (see, for example, Lake, 1989). The focus is usually on the fractional flow of oil and water, with emphasis on the physics of the flow (Walsh and Lake, 1989). The physics of two-phase flow is rarely combined with the chemistry of intraphase speciation and interphase mass transfer, especially when a gas phase is present.

This article examines geochemical phenomena coupled to two-phase flow, emphasizing the effects of concurrent aqueous and gas phase flow on mineral zonation. In particular, we focus on the wave behavior caused by either a flowing gas

phase created within the permeable medium or by an injected gas phase with potential for chemical interaction with the initial mineral phases.

Mathematical Development of Model

This section summarizes the equations for solving two-phase flow problems with significant mass transfer among the solid, aqueous and gas phases, induced by mineral dissolution and precipitation.

System description and assumptions

We consider a one-dimensional permeable medium with length L and unit cross-sectional area normal to flow. The medium consists of an inert solid, which occupies a constant fraction of the total volume and whose pores are filled with aqueous, soluble mineral or gaseous phases. We assume that all soluble minerals are stationary and that they occupy a very small fraction of the available void volume. In addition, we assume that all solids are incompressible which, combined with the assumption that soluble minerals have negligible volume, is equivalent to specifying constant porosity (void volume fraction) ϕ. Therefore, the sum of the volumes of the gas and aqueous phases per unit volume of medium is a constant. We will ignore capillary pressure, so the pressure of all phases is the same at a given location and time.

Chemical equilibrium

The local equilibrium assumption (LEA) is the basis for all chemical interactions in this study. The LEA allows the kinetics and local mass transfer rates for mineral dissolution and precipitation to be ignored and obviates the need for individual species balances. Mathematical formulations for geochemical transport problems, where the LEA has been relaxed, are given by Lichtner (1985).

Chemical equilibrium plays an integral part in the phenomena studied here, since it is the only mechanism for mass transfer between phases. For example, a chemical reaction describing calcite $CaCO_3(s)$ dissolution,

$$2H^+ + CaCO_3(s) \Leftrightarrow Ca^{++} + CO_2(g) + H_2O(aq),$$

expresses a net transfer of mass among the solid, aqueous and gas phases. It is through such interphase reactions that the chemistry is coupled to the physics of the flow.

We use the Villars-Cruise-Smith (VCS) algorithm for calculating chemical equilibrium because it is both robust and fast (Smith and Missen, 1982). The VCS algorithm efficiently solves the nonlinear algebraic equations describing the minimization of Gibbs free energy for a set of independent chemical reactions that completely specify the chemical system. See Novak (1990) for further discussion.

Overview of flow algorithm

This section describes the equations necessary to solve for compositions two-phase flow-through in permeable media when mass transfer between phases dominates the behavior. The solution scheme is based on the implicit-pressure/explicit-saturation (IMPES) method used frequently for simulating flows in petroleum reservoirs (Peaceman, 1977; Aziz and Settari, 1979).

Material balances in permeable media

We begin with a material balance on each of the I chemical elements in the medium:

$$\frac{\partial}{\partial t}[\phi(S_1C_{i1} + S_3C_{i3}) + (1-\phi)C_{i2}] + \frac{\partial}{\partial x}[C_{i1}u_1 + C_{i3}u_3] = 0 \qquad i = 1,\ldots,I \quad (1)$$

where u_j is the superficial (Darcy) velocity of phase j, S_j is the saturation (volume fraction) of phase j, and physical dispersion has been ignored. The subscripts 1, 2, and 3 refer to the aqueous, mineral, and gas phases, respectively. C_{ij} is the concentration of element i in phase j and has units of mass i per volume of phase j.

Summing Eq. 1 over the $i = 1,\ldots,I$ elements yields a material balance in terms of phase densities:

$$\frac{\partial}{\partial t}[\phi(S_1\rho_1 + S_3\rho_3)] + (1-\phi)\rho_2] + \frac{\partial}{\partial x}[\rho_1u_1 + \rho_3u_3] = 0 \quad (2)$$

where

$$\rho_j = \sum_{i=1}^{I} C_{ij}$$

Equation 2 separates into material balances on each phase when phase source terms, that is, *reaction terms*, are included, providing for constant porosity,

$$\phi\frac{\partial(S_j\rho_j)}{\partial t} + \frac{\partial(\rho_ju_j)}{\partial x} = r_j \quad j = 1,3 \quad (3a)$$

$$(1-\phi)\frac{\partial\rho_2}{\partial t} = r_2 \quad (3b)$$

where $r_1 + r_2 + r_3 = 0$, since mass transfer conserves total mass.

Overall material balance in terms of density and pressure

An overall material balance on the flowing phases in terms of density and pressure is achieved by expanding the time derivative in the gas- and aqueous-phase balances, Eq. 3a; and dividing by ρ_j and adding the aqueous- and gas-phase balances, it results in:

$$\sum_{j=1,3}\frac{S_j}{\rho_j}\frac{\partial\rho_j}{\partial t} + \sum_{j=1,3}\frac{1}{\phi\rho_j}\frac{\partial(\rho_ju_j)}{\partial x} = \sum_{j=1,3}\frac{r_j}{\rho_j\phi}. \quad (4)$$

This equation results through the simplification provided by the constraint $S_1 + S_3 = 1$.

Darcy's law provides a relationship between the superficial velocity of a phase and the pressure gradient in a permeable medium:

$$u_j = -\lambda_j\left(\frac{\partial P}{\partial x} + \rho_j g\right)$$

where g is the component of the gravitational acceleration vector parallel to the direction of the flow. The gravity term is included for completeness; and we will restrict our analysis to horizontal media from this point forward. The mobility of phase j, λ_j, is given by the equation:

$$\lambda_j = \frac{k k_{rj}}{\mu_j}$$

where k is the absolute permeability of the medium, k_{rj} is the relative permeability of phase j in the medium, and μ_j is the phase viscosity. The relative permeability is a property of the permeable medium and the fluids in the medium. Except for flows at very low interfacial tension, k_{rj} is usually considered a function of the S_j only (Lake, 1989). Substituting Darcy's law for phase velocity, Eq. 4 becomes the *pressure equation*:

$$\sum_{j=1,3}\frac{S_j}{\rho_j}\frac{\partial \rho_j}{\partial t} - \sum_{j=1,3}\frac{1}{\phi\rho_j}\frac{\partial}{\partial x}\left(\rho_j\lambda_j\frac{\partial P}{\partial x}\right) = \sum_{j=1,3}\frac{r_j}{\rho_j\phi}. \tag{5}$$

Finite-difference analog to the pressure equation

Finite differences are used to solve the partial differential equations on an equally-partitioned discretized domain. The domain is divided into N_s blocks. The center of each block is assigned an integer index ($k = 1,\ldots,N_s$), and the boundaries between blocks are assigned half-integer indices.

Time and space derivatives are approximated using backwards and implicit central finite differences, respectively, at time levels n and $n+1$, and spatial nodes k, $k+1/2$, and $k-1/2$. In finite difference form, Eq. 4 becomes:

$$\sum_{j=1,3}\frac{S_{jk}}{\rho_{jk}}\left(\frac{\rho_{jk}^{n+1}-\rho_{jk}^{n}}{\Delta t}\right) + \sum_{j=1,3}\frac{1}{\phi\rho_{jk}}\left(\frac{(\rho_j u_j)_{k+1/2}^{n+1}-(\rho_j u_j)_{k-1/2}^{n+1}}{\Delta x}\right) = \sum_{j=1,3}\frac{r_{jk}^{n+1}}{\rho_{jk}\phi} \quad k=1,\ldots,N_s \tag{6}$$

for all nodes in the discretized domain. Incorporating a finite difference analog to Darcy's law,

$$u_{k+1/2}^{n+1} = \frac{-\lambda_{jk+1/2}^{n+1}(P_{k+1}-P_k)^{n+1}}{\Delta x}$$

into Eq. 6, evaluating the as-yet-unsuperscripted densities at the $n+1$th level and the as-yet-unsuperscripted saturation at the nth time level, and rearranging give:

$$\sum_{j=1,3}\frac{\phi\Delta x^2 S_{jk}^{n}}{\Delta t}\left(\frac{\rho_{jk}^{n+1}-\rho_{jk}^{n}}{\rho_{jk}^{n+1}}\right) - \sum_{j=1,3}\frac{r_{jk}^{n+1}\Delta x^2}{\rho_{jk}^{n+1}} = \sum_{j=1,3}\frac{\rho_{jk+1/2}^{n+1}}{\rho_{jk}^{n+1}}\lambda_{jk+1/2}^{n+1}(P_{k+1}-P_k)^{n+1} - \sum_{j=1,3}\frac{\rho_{jk-1/2}^{n+1}}{\rho_{jk}^{n+1}}\lambda_{jk-1/2}^{n+1}(P_k-P_{k-1})^{n+1} \tag{7}$$

Equation 7 contains mobilities at time level $n+1$ which are unknown. We approximate the mobility at $n+1$ with the mobility at n, which is called explicit dating of saturation-dependent quantities. This assumption constrains the time step such that $\lambda_{jk\pm1/2}^{n}$ is approximately equal to $\lambda_{jk\pm1/2}^{n+1}$. Mobilities and densities at half-nodes in Eq. 7 are approximated using upstream weighting, so that $k-1/2$ becomes $k-1$ and $k+1/2$ becomes k. Peaceman (1977) has shown that weighting with any downstream character is unconditionally unstable in the absence of dispersion. By defining upstream weighting as above, we have implicitly assumed that flow is in the positive x direction only. Appropriate modifications must be made to allow for flow in the negative x direction.

Finite-difference analog to the flow (saturation) equations

Transport and chemical equilibriums are decoupled in the computational scheme outlined above, meaning that phases flow unchanged (with no source terms) from block to block at the beginning of each time step. After flow, equilibrium is calculated among phases, and the change in phase mass dictated by chemical equilibrium is the source/sink term. Other schemes for solving coupled systems of PDE's are discussed by Oran and Bori (1987).

The saturation equations, Eq. 3, can be thought of as volume balances because they dictate the phase volume fractions at time level $(n+1)$ in terms of phase volume fractions, velocities, and densities at time level n. The transport equations, Eq. 1, which sum to the saturation equation, then yield unequilibrated saturations which, when equilibrated (when the source terms are included), will satisfy the condition that the sum of the saturations is unity.

We apply the finite difference approximation to Eq. 3a, rearrange and divide it by density and porosity to achieve the equations for updating saturation:

$$S_{jk}^{n+1} = \frac{\rho_{jk}^{n}}{\rho_{jk}^{n+1}}S_{jk}^{n} - \frac{\Delta t}{\phi\Delta x}\left(\frac{\rho_{jk+1/2}^{n+1}}{\rho_{jk}^{n+1}}u_{jk+1/2}^{n+1} - \frac{\rho_{jk-1/2}^{n+1}}{\rho_{jk}^{n+1}}u_{jk-1/2}^{n+1}\right) \quad j=1,3. \tag{8}$$

Equation 8 again uses upstream weighting to approximate quantities evaluated at half nodes.

Transforming element transport equations to species transport equations

Transport equations written in terms of species concentrations are more useful computationally than balances on elements in problems with varying phase compositions. Thus, we transform Eq. 1 into equivalent balances on species. Species balances, rather than element balances, are needed because the VCS algorithm requires an approximation to species concentrations satisfying elemental abundances to begin the equilibrium calculation. However, element balances by phase and species balances are equivalent in the context of this article.

To obtain transport equations for species, we use the stoichiometric relationship:

$$C_{ij} = \sum_{m=1}^{M}\nu_{imj}\frac{n_{mj}}{MW_{mj}} \quad i=1,\ldots,I;\ j=1,\ldots,J \tag{9}$$

where n_{mj} is the concentration of species m in phase j in moles per volume of phase j, ν_{imj} is the stoichiometric coefficient of element i in species m in phase j, and MW_{mj} is the molecular weight of species m in phase j. By definition, species with concentration represented by n_{mj} can occur only in one phase. Therefore, the ν_{imj} vectors of constant j are orthogonal: $[\nu_{im1}]\cdot[\nu_{im2}]^T=[\nu_{im2}]\cdot[\nu_{im3}]^T=[\nu_{im1}]\cdot[\nu_{im3}]^T=0$. Substituting Eq. 9 into Eq. 1 and recognizing this orthogonality result in the species material balances:

$$\sum_{m=1}^{M}\frac{\nu_{imj}}{MW_{mj}}\left\{\frac{\partial}{\partial t}[\phi(S_j n_{mj})]+\frac{\partial}{\partial x}[n_{mj}u_j]\right\}=0 \quad j=1,3$$

$$\sum_{m=1}^{M}\frac{\nu_{im2}}{MW_{m2}}\left\{\frac{\partial}{\partial t}[(1-\phi)n_{m2}]\right\}=0$$

Because the stoichoimetric coefficients and molecular weights are independent constants, the summations drop out leaving:

$$\frac{\partial}{\partial t}[\phi(S_j n_{mj})]+\frac{\partial}{\partial x}[n_{mj}u_j]=0 \quad j=1,\ 3;\ m=1,\ldots M \tag{10a}$$

$$\frac{\partial}{\partial t}[(1-\phi)n_{m2}]=0 \qquad m=1,\ldots M \tag{10b}$$

The m index indicates applicability to all species; however, since species are phase-dependent inherently, one needs only sum over the species in the phase to which Eqs. 10a and 10b are being applied. Finite differencing consistent with that used previously results in the following equations for calculating transport:

$$(S_j n_{mj})_k^{n+1}=(S_j n_{mj})_k^n+\frac{\Delta t}{\phi\,\Delta x}\left(u_{jk-1/2}^{n+1}\,n_{mjk-1}^n-u_{jk+1/2}^{n+1}\,n_{mjk}^n\right)$$

$$m=1,\ldots,M \tag{11a}$$

$$n_{m2}^{n+1}=n_{m2}^n \qquad m=1,\ldots,M \tag{11b}$$

It might seem odd that Eq. 11b says that the mineral concentrations do not change over a time step. However, since minerals are stationary, they are completely independent of flow and thus change in response to changing aqueous and gas concentrations.

The differenced transport equations provide values for the total mole amounts of each species at the new time levels, but do not include any interphase equilibria. Equilibrium is calculated after transport using the VCS algorithm which minimizes the total Gibbs free energy of the chemical system in each grid block. The equilibrium concentrations of each species are calculated as a function of total element amounts (as represented by species) by the functionality:

$$n_{mj}^{n+1,e}=F(n_{11}^{n+1},\ n_{21}^{n+1},\ldots,n_{M1}^{n+1},\ n_{12}^{n+1},\ldots,\ n_{M2}^{n+1},\ n_{13}^{n+1},\ldots,n_{M3}^{n+1})$$

The equilibrated species concentrations in turn dictate the volume of each phase. When no mass changes phase, the equilibrium saturations are equal to those provided by Eq. 8. However, when mass does change phase through chemical reaction, the volume fractions in general will not be the same as those given by Eq. 8. Rather, there is a local source or sink of mass (and thus volume) to each phase caused by the chemical reactions; the change in volume is because of different phase densities. The amount of mass that has change phase because of chemical reaction in each grid block is given by:

$$r_{jk}^{n+1}=\sum_{m=1}^{M}MW_{mj}(n_{mjk}^{n+1,e}-n_{mjk}^{n+1}) \tag{12}$$

Boundary and initial conditions

The pressure equation requires two boundary conditions and an initial condition for unique solution; we chose to specify a flux into the medium ($x=0$), a pressure at the end of the medium ($x=L$), and an initial pressure profile. For the transport equations, the composition flowing into the domain and the initial compositions throughout the domain were specified.

Solution techniques used for pressure/flow equations

We have developed a geochemical flow simulator, called GEOFLOW, to solve the equations presented here. [GEOFLOW also solves other geochemical flow/diffusion problems. See Novak (1990) and Novak et al. (1989).] The iterative calculation procedure for solving the coupled discretized PDS's and equilibrium equation is as follows. At the beginning of a time step, the amount of mass changing phase is unknown, so iteration begins by assuming no mass changes phase, that is, by approximating $r_{jk}^{n+1}=0$. The pressure equation is solved, Eq. 7, species are transported using Eqs. 11a and 11b, equilibrium is calculated, and the phase source terms are approximated with Eq. 12. The newly calculated phase source terms are substituted into Eq. 7, and the cycle is repeated until the pressures no longer change. Figure 1 summarizes the two-phase calculation scheme for a single time step. For the examples presented, convergence of the $L2$ norm of the pressure to $<10^{-6}$ usually occurred within six to ten iterations using this successive substitution scheme.

Summary of numerical algorithm

We have expanded the IMPES method to allow species to transfer among phases and then to react to form different species. This method can be used to analyze systems, where a gas phase is produced by aqueous-mineral reactions and where a gaseous species is consumed by aqueous-mineral-gas reactions, as is demonstrated below.

Examples

The following two examples explain the two-phase flow solutions from the GEOFLOW simulator:

1. Hydrochloric acid injection into a medium containing calcite and iron(II) hydroxide, $CaCO_3$(s)/$Fe(OH)_2$(s), demonstrates that a flowing gas phase can be produced by aqueous-mineral reaction and can change the minerals in the medium far downstream of the aqueous-phase tracer wave. The tracer wave velocity also can be significantly increased by *in situ* gas concentration, relative to the analogous system without gas generation.

2. The stripping of hydrogen sulfide H_2S(g) is modeled from

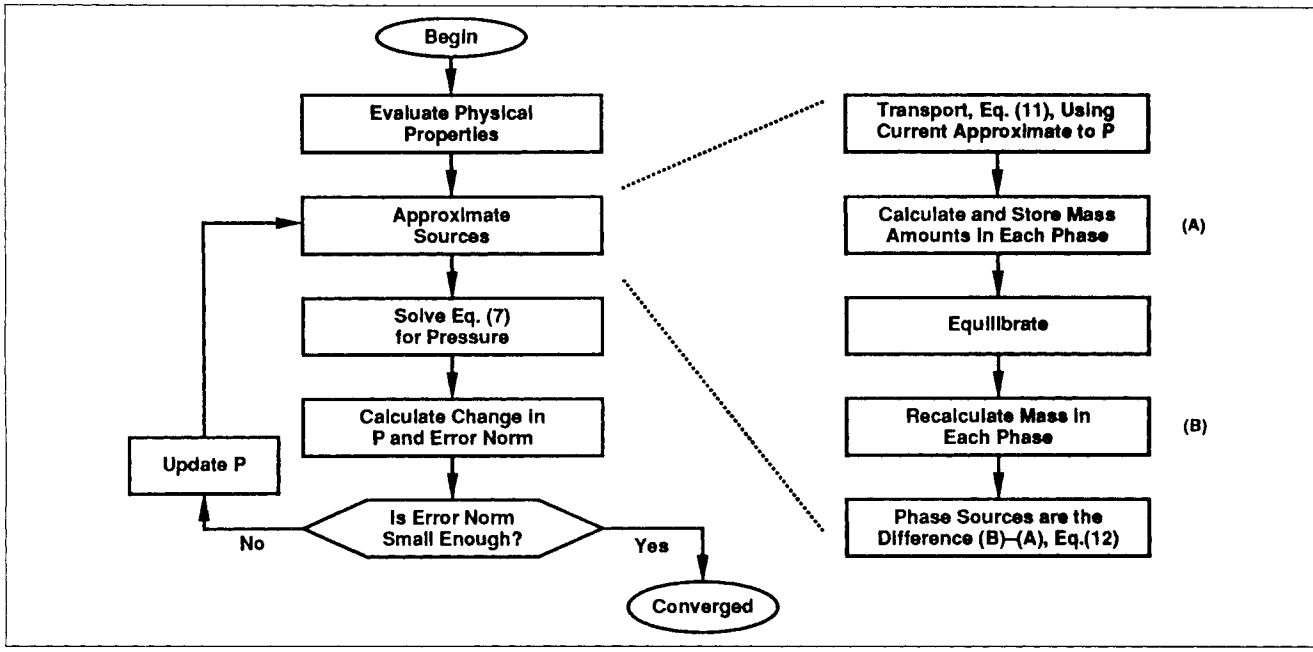

Figure 1. Pressure calculating procedure for a single time step.

carbon dioxide $CO_2(g)$ injected into a permeable medium initially containing siderite, $FeCO_3(s)$.

The gas phase in both examples is considered to be incompressible. We ignore redox reactions, so iron remains in the +II oxidation state and sulfur as −II throughout. The chemical species in the examples are listed in Table 1 and phase properties are in Table 2. Free energy of formation data was obtained from Garrels and Christ (1965), and activity corrections were assumed negligible.

We present results using two types of graphs: *distance-time diagrams* represent the propagation of each wave as a straight line radiating from the origin and *profiles* show concentration or saturation as a function of distance at fixed time. Distance x_D is expressed as a fraction of the total medium length, and time t_D is the total volume of fluid injected up to time t as a fraction of the medium's pore volume. In these dimensionless space and time coordinates, wave velocities are also dimensionless, being normalized by the injected fluid velocity. Three types of waves (changes in saturation or concentration) can occur: shock waves (also called sharpening waves) are abrupt changes and remain abrupt; indifferent waves are gradual changes that spread out as they travel due to dispersion (spreading is proportional to the square root of time); and spreading waves become more diffuse as they propagate due to physical processes other than dispersion (spreading is proportional to time).

Table 1. Chemical Species in the Calcite Dissolution and $H_2S(g)/CO_2(g)$ Injection Examples*

Aqueous	Mineral		Gas	
H_2O	$FeCO_3(s)$		$CO_2(g)$	
H_2CO_3	$Fe(OH)_2(s)$		$H_2S(g)$	[2]
HCO_3^-	$CaCO_3(s)$	[1]		
$CO_3^=$	$CaO(s)$	[1]		
Cl^-	$Ca(OH)_2(s)$	[1]		
H^+	$FeS(s)$	[2]		
OH^-	$FeO(s)$	[2]		
Fe^{++}				
Ca^{++}	[1]			
H_2S	[2]			
HS^-	[2]			
$S^=$	[2]			

*Species followed by [1] are in calcite dissolution example only; species followed by [2] are in the $H_2S(g)/CO_2(g)$ injection example only; and all other species are in both examples.

Calcite dissolution and carbon dioxide formation, converting all initial $Fe(OH)_2(s)$ to $FeCO_3(s)$

The calcite dissolution example shows the effect that a flowing gas phase can have on minerals present in a medium. Initially, the domain contains 0.04 mol $Fe(OH)_2(s)$/L pore volume and an excess of calcite, $CaCO_3(s)$. The system is per-

Table 2. Physical Properties in the Calcite Dissolution and $H_2S(g)/CO_2(g)$ Injection Examples

	Calcite Dissolution	$H_2S(g)/CO_2(g)$ Injection
ρ_1 (g/cm^3)	1.0	1.0
ρ_3 (g/cm^3)	0.09	0.9
μ_1 (mPa·s)	1.0	1.0
μ_3 (mPa·s)	0.1	0.1
Aqueous-Phase Residual Saturation	0.0	0.20
Gas-Phase Residual Saturation	0.0	0.10
Aqueous-Phase Relative Permeability	S_1	$\frac{S_1 - S_{1r}}{1 - S_{1r} - S_{3r}}$
Gas-Phase Relative Permeability	S_3	$\frac{S_3 - S_{3r}}{1 - S_{1r} - S_{3r}}$

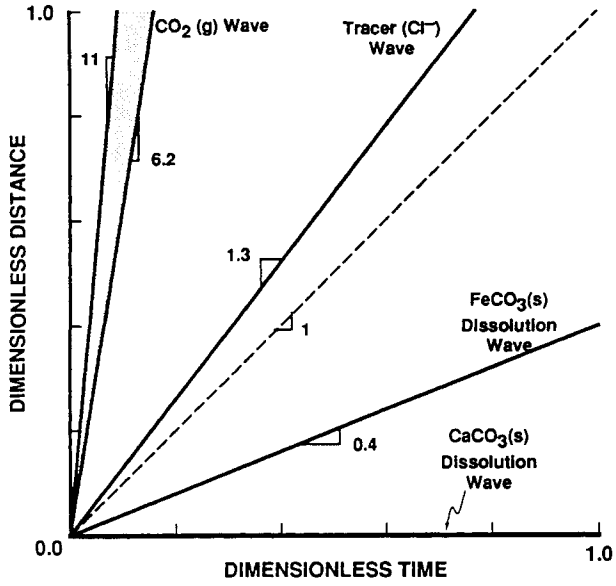

Figure 2. Distance time for calcite/iron(II) hydroxide.

It shows spreading CO_2(g) wave (shaded) at which $Fe(OH)_2$(s) is converted to $FeCO_3$(s), a tracer wave, a $FeCO_3$(s) dissolution wave, and a $CaCO_3$(s) dissolution wave.

turbed by injection of 10-M HCl, which initiates the four waves shown in the distance-time diagram of Figure 2.

The acid causes calcite dissolution and carbon dioxide gas formation. Because of its low viscosity, the gas is much more mobile than the aqueous phase, so it flows rapidly through the medium resulting in a spreading wave with a shock at the downstream end of the wave. The specific (dimensionless) velocities in Figure 2 are those where the gas saturation is 5% and 95% of the total saturation change in the spreading portion of the wave. The leading edge of the gas wave increases the acidity and total dissolved carbon dioxide concentration of the initial water, which converts all the $Fe(OH)_2$(s) initially present to $FeCO_3$(s). The gas achieves a saturation of $S_3 = 0.13$ upstream of the spreading wave, which is maintained up to the gas source, the calcite dissolution wave.

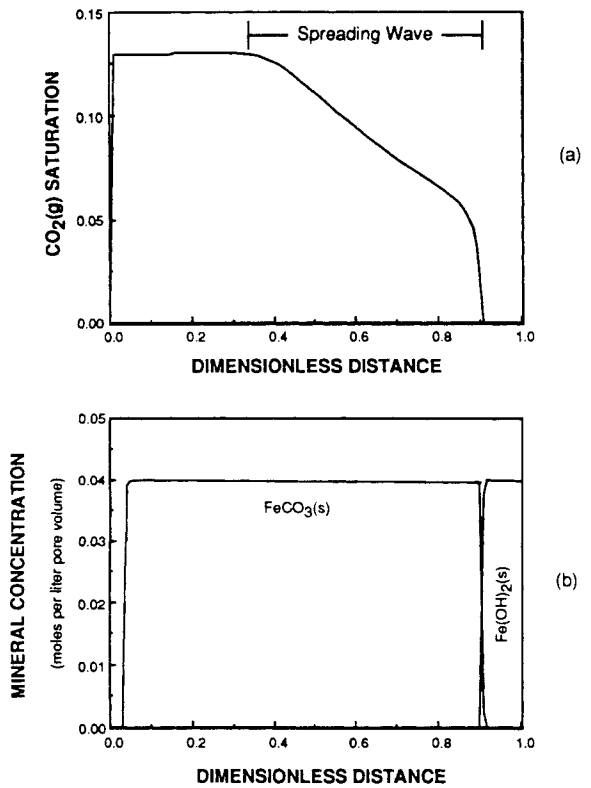

Figure 3. (a) Carbon dioxide gas saturation profile; (b) $Fe(OH)_2$(s) and $FeCO_3$(s) profiles for calcite/iron(II) hydroxide at $t_D = 0.069$.

Figure 3a shows the gas saturation profile at $t_D = 0.069$. The abrupt change, at $x_D = 0.9$, reflects carbon dioxide being taken up by the conversion of $Fe(OH)_2$(s) to $FeCO_3$(s) in Figure 3b. If the gas phase were not being taken into the mineral phase (as would be the case with no chemical reaction/interaction), the gas saturation curve would continue to spread, gradually decreasing to zero at the leading edge, instead of decreasing in an apparent shock as the figure illustrates.

The tracer wave moves with dimensionless velocity $v_T = 1.3$ (Figure 2), significantly faster than the tracer velocity of unity in single-phase problems. This increase in velocity reflects the substantial effect that the *in situ* production of gas can have on the rate of wave propagation in the aqueous phase. The tracer moves faster because the gas has a much larger volume than the aqueous and mineral species that react to form the gas. This volume blocks off much of the otherwise accessible pore space, allowing the aqueous phase and the tracer within it to move faster than in single-phase flow.

The third wave is the siderite dissolution wave. Siderite, not present initially, is formed when the gas phase comes into contact with the $Fe(OH)_2$(s) initially in the medium. Figure 3b shows both the $Fe(OH)_2$(s) to $FeCO_3$(s) dissolution/precipitation wave and the siderite dissolution wave near $x_D = 0.04$.

The calcite dissolution wave is the slowest moving wave in the system. Since calcite is present in excess, this wave moves with a negligibly small velocity. Calcite does play an important role in the process, however, because $CaCO_3$(s) dissolution is the source of the flowing CO_2(g) gas. Calcite also directly influences chemical compositions throughout the medium because its presence constrains aqueous-phase concentrations through local equilibrium.

An important difference between the behavior of single-phase and two-phase problems is that the downstream equilibrium condition (DEC) (Walsh et al., 1984) does not hold everywhere as it does in one-phase flow problems. The DEC dictates that the aqueous phase downstream of the dissolution/precipitation wave is in equilibrium with the minerals upstream of the wave, regardless of whether the upstream minerals are present in the downstream region. Figure 4 is a profile of the solubility quotient for siderite for the calcite dissolution example. Comparing Figures 3 and 4 shows that the solubility product of siderite (indicated on the figure) holds only where siderite is present, between $x_D \approx 0.04$ to $x_D \approx 0.90$, and not downstream of the $Fe(OH)_2$(s) dissolution/$FeCO_3$(s) precipitation wave. Thus, the DEC does not apply to this wave.

The DEC fails here because this wave is downstream of the aqueous tracer wave: it moves faster than the aqueous phase which carries the equilibrium information. In one-phase transport problems, the tracer wave is the fastest wave, thus there can be no waves aheads of the tracer. Any dissolution/pre-

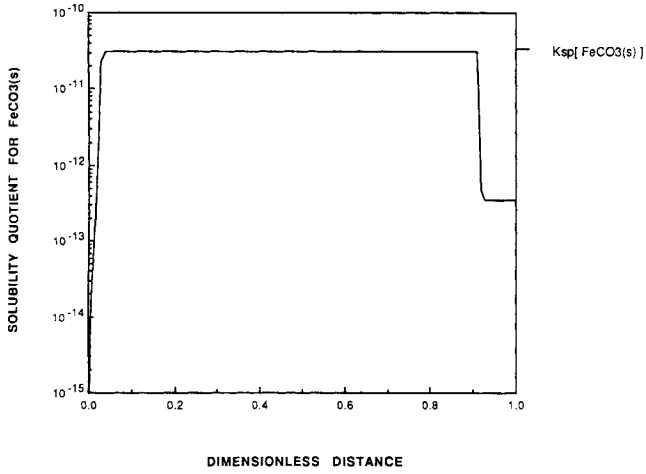

Figure 4. Solubility quotient vs. dimensionless distance at $t_D = 0.069$ for calcite/iron(II) hydroxide.

Solubility product is satisfied only where $FeCO_3(s)$ is present, not downstream of the $Fe(OH)_2(s)$ dissolution/$FeCO_3(s)$ precipitation wave at $x_D = 0.9$.

cipitation wave that moves faster than the tracer velocity, such as the iron(II) hydroxide to siderite wave of Figure 3, need not satisfy the DEC because the dissolution/precipitation wave travels ahead of the aqueous phase.

Metasomatic stripping of $H_2S(g)$ from injected $CO_2(g)$

The second example models the response of a siderite-rich medium to injected carbon dioxide contaminated with hydrogen sulfide, a gas composition that has been used in enhanced oil recovery (Rowe et al., 1982).

The medium initially contains $FeCO_3(s)$ at a concentration of 0.5 mol/L pore volume and an aqueous phase in equilibrium with this mineral. A gas mixture of 90 mol% carbon dioxide

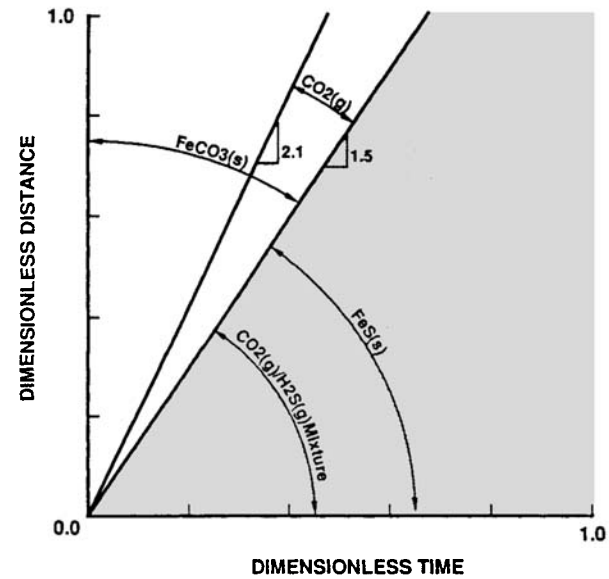

Figure 5. Distance time for the $CO_2(g)/H_2S(g)$.

It shows a $CO_2(g)$ wave, a $FeCO_3(s)$ dissolution/$FeS(s)$ precipitation wave, and a spreading $CO_2(g)/H_2S(g)$ wave (shaded).

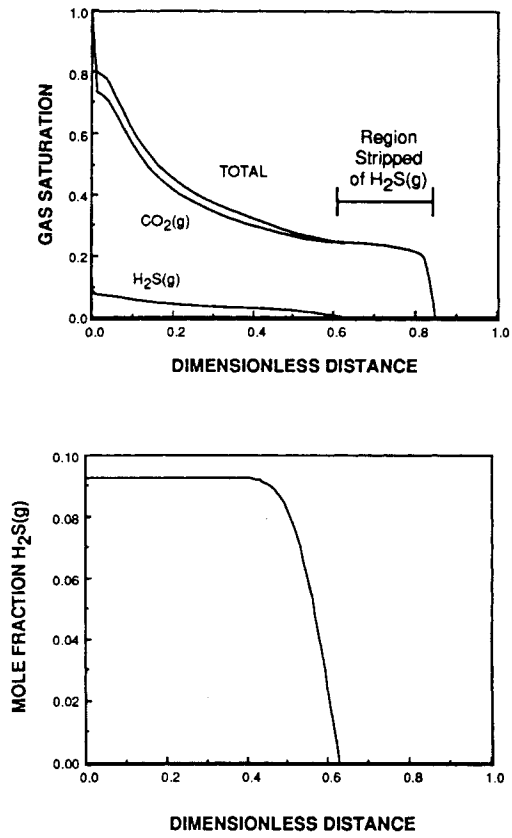

Figure 6. (a) Carbon dioxide, hydrogen sulfide, and total gas saturation profiles; (b) mole fraction of $H_2S(g)$ in the gas phase vs. dimensionless distance for the $CO_2(g)/H_2S(g)$ example at $t_D = 0.417$.

gas with 10 mol% hydrogen sulfide, mixed with about 2 vol.% water, is injected. (The water is present because the VCS algorithm, as implemented, requires an aqueous phase. When the gas and aqueous phases are equilibrated, the gas phase contains about 9.3 mol% H_2S.) This small quantity of injected water does little to the ensuing wave patterns. Water and gas are injected together frequently in enhanced oil recovery (Rowe et al., 1982). The injected gas and water create the wave pattern shown in the distance-time diagram of Figure 5.

The waves in this example, from fastest to slowest, are as follows. A carbon dioxide gas wave in the fastest, with a specific velocity of about 2.1. Upstream of this wave is another rather fast wave, where $H_2S(g)$ leaves the gas phase and converts all remaining siderite (and some of the Fe^{2+} in solution) into FeS(s). Next are the aqueous tracer and the FeS(s) dissolution waves, which move with velocities that are so small that they are unresolved at the time depicted in the figures. (The dimensionless time is based on volume injected, which is primarily gas in this example. The aqueous-tracer, wave-specific velocity is about 0.02 in this case.)

The gas saturation and the mole fraction $H_2S(g)$ profiles are plotted in Figures 6a and 6b at $t_D = 0.417$. The gas saturation decreases abruptly to zero at the leading edge ($x_D \approx 0.85$) of the gas wave because $CO_2(g)$ is being taken into the mineral phase as in the previous example. Only $CO_2(g)$ is present in the gas phase immediately upstream of this shock, as can be

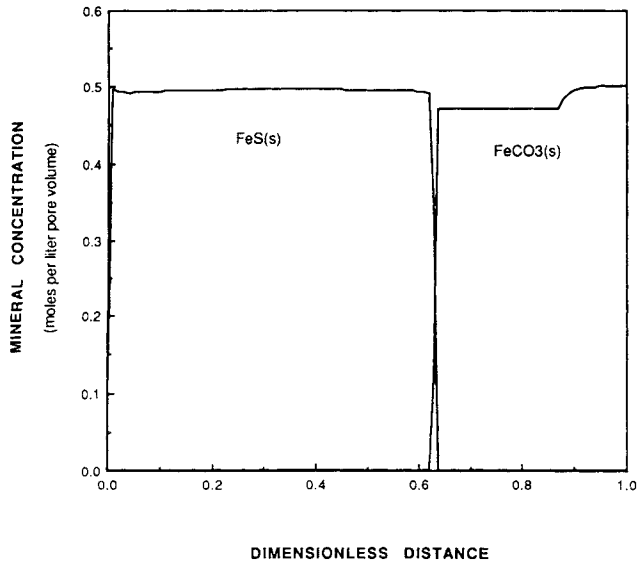

Figure 7. $FeCO_3$(s) and FeS(s) profiles for CO_2(g)/H_2S(g) at $t_D = 0.417$.

seen from the profile of mole fraction H_2S(g). The gas composition is constant behind the H_2S(g)/FeS(s) wave at $x_D \approx 0.4$, the wave where the H_2S is being stripped from the gas phase. The gas saturation decreases from 98 vol.% in the injected condition to 80% just inside the domain because there is a 20% residual water saturation.

The $FeCO_3$ profile in Figure 7 shows that the mineral concentration decreases when the gas phase is first in contact with the mineral at $x_D \approx 0.85$. When CO_2(g) contacts the initial aqueous phase, some CO_2(g) dissolves and increases the acidity of the aqueous phase by forming bicarbonate:

$$CO_2(g) + H_2O \Leftrightarrow H^+ + HCO_3^-$$

which causes additional $FeCO_3$ to dissolve through the reaction:

$$FeCO_3(s) + H^+ \Leftrightarrow Fe^{++} + HCO_3^-$$

Such partial dissolution waves have not been observed in simulations of single-phase transport (Novak et al., 1988).

Although not plotted for this example, the DEC does not hold for the $FeCO_3$(s) to FeS(s) transition; and this wave also moves faster than the aqueous tracer velocity.

Conclusions

We have modified the implicit pressure, explicit saturation (IMPES) algorithm by incorporating phase source terms coupled with chemical equilibrium to calculate metasomatic responses in media undergoing simultaneous gas and aqueous-phase flow. The two-phase transport system has much in common with single-phase transport, as described in earlier work, and with nonreactive, immiscible flows. However, the inclusion of a chemically-reactive, mobile gas phase causes the following differences between these two extremes.

1. Chemical reactions between an aqueous phase and resident minerals can cause a gas phase to form, and the gas phase can then flow.

2. As in nonreactive flows, the gas phase flows much faster than the aqueous phase in a spreading wave. Unlike nonreactive flow, the reacting gas phase can alter the medium's mineral state well ahead of the tracer wave, and these chemical reactions can change the shape of the displacement front. A shock can now proceed a spreading wave.

3. A reactive gas phase can cause partial dissolution of a resident mineral. This does not happen in single-phase flow; and a mineral either does not dissolve, dissolves completely, or changes concentration due to the dissolution of another mineral at the same wave.

4. The downstream equilibrium condition fails for dissolution/precipitation waves that propagate faster than the aqueous phase. All such waves involve the gas phase, because they would otherwise be moving with a velocity less than the tracer velocity. The DEC still applies to waves slower than the tracer wave.

The most practical result of this work perhaps is that it is possible for minor components to be stripped from a carrier gas phase through dissolution/precipitation reactions. This observation has implications for air stripping of aquifer pollutants and for the need for pre-injection purification of gases used in enhanced oil recovery.

Notation

C_{ij} = mass concentration of element i in phase j
k = absolute permeability
k_{rj} = relative permeability of phase j
L = length of medium
n_{mj} = molar concentration of species m in phase j
N_s = number of spatial nodes in the discretized domain
P = pressure
r_j = phase source term, see Eq. 3
r_{jk} = discretized phase source term
S_j = saturation (volume fraction) of phase j
t = time
t_D = dimensionless time
u_j = superficial velocity of phase j
v = wave velocity
v_T = tracer wave velocity
x = position
x_D = dimensionless position

Greek letters

Δt = time step for numerical integration
Δx = space step for numerical integration
λ_j = mobility of phase j
μ_j = viscosity of phase j
ν_{imj} = stoichiometric coefficient of element i in species m in phase j
ρ_j = density of phase j
ϕ = porosity

Subscripts

i = ith element
j = quantity in the jth phase ($j=1$ is aqueous, $j=2$ is mineral, $j=3$ is gas)
k = grid block index for discretized domain
m = mth chemical species

Superscript

n = time level index

Literature Cited

Aziz, K., and A. Settari, *Petroleum Reservoir Simulation*, Applied Science, London (1979).

Bryant, S. L., R. S. Schechter, and L. W. Lake, "Interactions of Precipitation/Dissolution Waves and Ion Exchange in Flow through Permeable Media," *AIChE J.*, **32**, 751 (May, 1986).

Bryant, S. L., R. S. Schechter, and L. W. Lake, "Mineral Sequences in Precipitation/Dissolution Waves," *AIChE J.*, **33**, 1271 (Aug., 1987).

Dria, M. A., L. W. Lake, and R. S. Schechter, "An Analysis of Reservoir Chemical Treatments," *SPE Prod. Eng.*, 52 (Feb., 1988).

Garrels, R. M., and C. L. Christ, *Solutions, Minerals, and Equilibria*, Harper and Row, New York (1965).

Helfferich, F. G., "The Theory of Precipitation/Dissolution Waves," *AIChE J.*, **35**, 75 (Jan., 1989).

Kirkner, D. J., and H. Reeves, "Multicomponent Mass Transport With Homogeneous and Heterogeneous Chemical Reaction—Effect of the Chemistry on the Choice of Numerical Algorithm: 1. Theory," *Water Resour. Res.*, **24**(10), 1719 (1988).

Lake, L. W., *Enhanced Oil Recovery*, Prentice-Hall, Englewood Cliffs, NJ (1989).

Lichtner, P. C., "Continuum Model for Simultaneous Chemical Reactions and Mass Transport in Hydrothermal Systems," *Geochim. et Cosmochim. Acta*, **49**, 779 (1985).

Lichtner, P. C., "The Quasistationary State Approximation to Fluid/Rock Reaction: Local Equilibrium Revisited," *Advances in Physical Geochemistry, Vol. 8, Diffusion, Atomic Ordering, and Mass Transport*, p. 452, J. Ganguly, ed., Springer-Verlag (1991).

Novak, C. F., R. S. Schechter, and L. W. Lake, "Rule-based Mineral Sequences in Geochemical Flow Processes," *AIChE J.*, **34**, 1607 (Oct., 1988).

Novak, C. F., R. S. Schechter, and L. W. Lake, " Diffusion and Solid Dissolution/Precipitation in Permeable Media," *AIChE J.*, **35**, 1057 (July, 1989).

Novak, C. F., "Metasomatic Patterns Produced by Infiltration or Diffusion in Permeable Media," PhD Diss., Univ. of Texas at Austin (1990).

Oran, E. S., and J. P. Boris, *Numerical Simulation of Reactive Flows*, Elsevier, New York (1987).

Ortoleva, P., E. Merino, C. Moore, and J. Chadam, "Geochemical Self-Organization: I. Reaction-Transport Feedbacks and Modeling Approach," *Amer. J. Sci.*, **287**, 979 (1987).

Peaceman, D. W., *Fundamentals of Numerical Reservoir Simulation*, Elsevier, New York (1977).

Rege, S. D., and H. S. Fogler, "Competition Among Flow, Dissolution, and Precipitation in Porous Media," *AIChE J.*, **35**, 1177 (1989).

Rowe, H. G., S. D. York, and J. C. Ader, "Slaughter Estate Unit Tertiary Pilot Performance," *J. Pet. Tech.* **34**, 613 (Mar., 1982).

Rubin, J., "Transport of Reacting Solutes in Porous Media: Relation Between Mathematical Nature of Problem Formulation and Chemical Nature of Reactions," *Water Resour. Res.*, **19**(5), 1231 (1983).

Schechter, R. S., S. L. Bryant, and L. W. Lake, "Isotherm-free Chromatography: Propagation of Precipitation/Dissolution Waves," *Chem. Eng. Commun.*, **58**, 353 (1987).

Simmons, D. M., "A Study of the Reactive Flow of EDTA in Berea Sandstone," MS Thesis, Univ. of Texas at Austin (1988).

Smith, W. R., and R. W. Missen, *Chemical Reaction Equilibrium Analysis: Theory and Algorithms*, Wiley, New York (1982).

Walsh, M. P., L. W. Lake, and R. S. Schechter, "A Description of Chemical Precipitation Mechanisms and Their Role in Formation Damage During Stimulation by Hydrofluoric Acid," *J. Pet. Tech.*, **34**, 2097 (Sept., 1982).

Walsh, M. P., S. L. Bryant, R. S. Schechter, and L. W. Lake, "Precipitation and Dissolution of Solids Attending Flow through Porous Media," *AIChE J.*, **30**, 217 (Mar., 1984).

Walsh, M. P., and L. W. Lake, "Applying Fractional Flow Theory to Solvent Flooding and Chase Fluids," *J. Pet. Sci. Eng.*, **2**, 281 (1989).

Manuscript received Apr. 24, 1991, and revision received Sept. 26, 1991.